



One-pot catalytic reaction to produce high-carbon-number dimeric deoxygenated hydrocarbons from lignin-derived monophenyl vanillin using Al₂O₃-cogelled Ru nanoparticles



Indri Yati ^{a,b,1}, Adid Ade Dwiatmoko ^{a,c,1}, Ji Sun Yoon ^a, Jae-Wook Choi ^a, Dong Jin Suh ^{a,c,d}, Jungho Jae ^{a,b}, Jeong-Myeong Ha ^{a,b,d,*}

^a Clean Energy Research Center, Korea Institute of Science and Technology, Seoul 02792, Republic of Korea

^b Department of Clean Energy and Chemical Engineering, Korea University of Science and Technology, Daejeon 34113, Republic of Korea

^c Department of Green Process and System Engineering, Korea University of Science and Technology, Daejeon 34113, Republic of Korea

^d Green School (Graduate School of Energy and Environment), Korea University, Seoul 02841, Republic of Korea

ARTICLE INFO

Article history:

Received 4 April 2016

Received in revised form 15 July 2016

Accepted 17 July 2016

Available online 18 July 2016

Keywords:

Vanillin

Ruthenium

Alumina

Hydrodeoxygenation

Condensation

ABSTRACT

Al₂O₃-cogelled Ru nanoparticle (Ru@Al) catalyst was prepared by a one-pot in-situ alumina gelation method using a PVP-stabilized Ru colloid solution. The Ru@Al catalyst exhibited excellent catalytic activity during the liquid-phase hydrodeoxygenation of vanillin, demonstrating 100% conversion, as well as significantly higher yields of fully deoxygenated compounds compared to other conventional alumina-supported Ru catalysts. We also observed better selectivity to deoxygenated dimers with the Ru@Al catalyst. The improved catalytic selectivity was attributed to the hypothesized three-dimensional structures of Al₂O₃ surrounding the Ru nanoparticles, which improved the two-step reaction, containing the dimerization of the phenolic compounds and the hydrodeoxygenation of phenolic dimers to produce deoxygenated high-carbon-number hydrocarbons.

© 2016 Elsevier B.V. All rights reserved.

1. Introduction

The production of hydrocarbon fuels from biomass is a next major challenge in the effort to develop advanced biofuels, and the thermolysis of lignocellulosic biomass appears to be a practical method to produce bio-oils, precursors of petroleum, to replace hydrocarbon fuels [1–3]. In order to produce petroleum-like hydrocarbon fuels, the oxygen atoms in bio-oils must be removed, which has been achieved by catalytic hydrodeoxygenation (HDO) [4–6]. Along with HDO, the production of high-carbon-number hydrocarbons has been studied in order to produce high-energy-density fuels to be blended with diesel fuels [7,8]. Alkylation [9], aldol condensation [7,10], and other condensation processes [8] have been suggested in the literature.

For the production of high-carbon-number hydrocarbons during the HDO of small phenolic compounds, the condensation of small molecules on acid catalysts is investigated in this study.

Because the formation of monomeric deoxygenated hydrocarbons from lignin-derived small-molecule phenolic compounds has been observed when bifunctional catalysts of metals supported on solid acids were used [11–19], a new catalyst design was required to produce high-carbon-number deoxygenated hydrocarbons and prevent the formation of oligomers.

In our previous study, we prepared sintering-resistant Pt nanoparticles, which were strongly interacted with alumina nanorods (Pt@Al₂O₃), by a simple preparation method, with which a highly active water gas shift reaction was performed without significant sintering of the Pt nanoparticles [20]. With a similar approach, herein we report that a prepared Al₂O₃-cogelled Ru nanoparticle (Ru@Al) catalyst exhibits interesting performance during the hydrodeoxygenation of vanillin at 40 bar and 270 °C in an aqueous solution. Vanillin, 4-hydroxy-3-methoxybenzaldehyde, was selected as a small-molecule phenolic compound to represent lignin-derived small molecules in this study. It contains three oxygenated functional groups: aldehyde, ether, and hydroxyl [21]. The HDO of vanillin has been reported to produce vanillin alcohol, *p*-creosol, and guaiacol as major products using supported noble-metal catalysts of Pd, Ru, and Au [21–25]. Moreover, we previously reported that the activity of the Ru catalyst on the HDO of lignin monomer was higher than those of the Pd and

* Corresponding author at: Clean Energy Research Center, Korea Institute of Science and Technology, Seoul 02792, Republic of Korea.

E-mail address: jmha@kist.re.kr (J.-M. Ha).

¹ These authors equally contribute to this work.

Pt catalysts [11,26]. In this study, we observe that the catalysis using Ru@Al is more selective toward the formation of dimeric hydrocarbon compared to other conventionally impregnated alumina-supported Ru catalysts (Ru/Al₂O₃) which are more selective toward monomeric hydrocarbons. The reaction pathway is suggested for the hydrodeoxygénéation of vanillin, and the formation of dimeric hydrocarbons on Ru@Al was discussed based on the structures of the catalysts. The observations noted with Ru@Al may apply to the production of high-carbon-number hydrocarbon fuels from lignocellulose.

2. Experimental

2.1. Materials

All chemicals were used without further purification. Ruthenium(III) chloride hydrate (RuCl₃·nH₂O), polyvinylpyrrolidone (PVP), aluminum tri-sec-butoxide [Al(OCH(CH₃)C₂H₅)₃, 97%], and vanillin were purchased from Aldrich (Milwaukee, WI, USA). Ethylene glycol was purchased from Junsei Chemical (Tokyo, Japan). γ-Al₂O₃ was purchased from Alfa Aesar (Ward Hill, MA, USA). Deionized water (18.2 MΩ cm) was prepared using an aqua-MAX Ultra 370 water purification system (Young Lin Instrument, Anyang, Korea).

2.2. Preparation of catalysts

PVP-stabilized Ru nanoparticles were prepared by modifying a method described in the literature [27]. RuCl₃·nH₂O (0.0285 g, 0.14 mmol) dissolved in DI water (0.61 mL) was added to PVP (0.252 g) dissolved in ethylene glycol (19 mL). The mixture was then heated for 1 h at 190 °C to produce PVP-stabilized Ru NPs. Ru@Al was prepared by polymerizing alumina precursors in the presence of PVP-stabilized Ru NPs. Al[OCH(CH₃)C₂H₅]₃ (3.29 mL, 13 mmol) dissolved in ethanol (130 mL) was added to a previously prepared colloidal solution of Ru nanoparticles and the mixture was stirred for two days at room temperature. The resulting mixture was centrifuged with an addition of acetone, washed with acetone, and dried in air for 16 h at 100 °C. The mixture was further calcined in air for 2 h at 400 °C, reduced under a H₂ flow for 4 h at 400 °C, and then passivated with a 0.5% O₂/N₂ (v/v) flow for 30 min at room temperature to be stored under ambient conditions. Alumina prepared in the absence of Ru (FreeAl) was synthesized with the same procedure described for the synthesis of Ru@Al, only without the addition of RuCl₃·nH₂O. Alumina aerogel (AeroAl) was prepared following the method described in our previous work [8]. Ru NPs supported on FreeAl, AeroAl, and γ-Al₂O₃ (Ru/FreeAl, Ru/AeroAl, and Ru/γ-Al₂O₃, respectively) were prepared by adding alumina as a support (0.658 g) to a previously prepared colloidal solution of PVP-stabilized Ru nanoparticles, with the mixture then stirred for two days at room temperature. The produced mixture was centrifuged with the addition of acetone, washed with acetone, and dried in air for 16 h at 100 °C. The mixture was further calcined in air for 2 h at 400 °C, reduced under a H₂ flow for 4 h at 400 °C, and then passivated with a 0.5% O₂/N₂ (v/v) flow for 30 min at room temperature to be stored under ambient conditions. The metal loadings of all catalysts prepared in this study were 2 wt%.

2.3. Characterization of catalysts

The powder X-ray diffraction (XRD) results were obtained using a Rigaku Miniflex-II X-ray diffractometer (Tokyo, Japan) equipped with Cu Kα_{ave} ($\lambda = 0.15418 \text{ nm}$) at 30 kV and 15 mA. High-resolution transmission electron microscopy (HR-TEM) images and high-angle annular dark-field scanning transmission electron microscopy (HAADF-STEM) images were obtained using a

Tecnai G2 F20 instrument at 200 kV. A SEM analysis with EDX mapping was performed using an FE-SEM Hitachi S-4200 instrument operating at 30 kV. N₂-Physisorption results were obtained using a Micromeritics ASAP 2020 instrument. NH₃-temperature-programmed desorption/mass spectroscopy (NH₃-TPD/MS), H₂-TPD/MS, and CO-chemisorption results were obtained using a BELCAT-B catalyst analyzer (BEL Japan, Inc.) equipped with a thermal conductivity detector (TCD) and a mass spectrometer (MS) with an appropriate pretreatment (Table S1). X-ray photoelectron spectroscopy (XPS) was performed using a PHI 5000 Versa Probe (Ulvac-PHI) with a monochromatized microfocused Al X-ray source. The binding energy was calibrated with C 1s at 284.6 eV.

2.4. Catalysis

The catalytic hydrodeoxygénéation of vanillin was performed in a stainless steel autoclave reactor (~100 mL). In a typical reaction procedure, vanillin (1.8 mmol), water (30 mL), and a solid catalyst (50 mg) were added to the reactor. After flushing with N₂ gas, the reactor was pressurized to 40 bar with H₂ at room temperature. The reaction was performed at 270 °C for 2 h with an agitation rate of 800 rpm. After the reaction, the reactor was cooled to room temperature and the mixture was extracted with ethyl acetate. The catalyst powder was removed and the liquid product was collected. The extracted products were analyzed using a gas chromatograph-mass spectrometer combination (GC/MS, Agilent 7890A with 5975C inert MS XLD) with a HP-5 capillary column (60 m × 0.25 mm × 250 μm). The conversion of vanillin, product selectivity, product yield, and the oxygen removal are defined as follows:

$$\text{Conversion of vanillin(mol\%)} = (C_0 - C_f)/(C_0) \times 100$$

$$\text{Selectivity to products(mol\%)} = (C_i)/(C_0 - C_f) \times 100$$

$$\text{Yield of products(mol\%)} = (C_i)/(C_0) \times 100$$

$$\begin{aligned} \text{Oxygen removal} &= [(Yield of 0-Os) + 2/3 \times (Yield of 1-Os) \\ &\quad + 1/3 \times (Yield of 2-Os)] \end{aligned}$$

where C₀ and C_f are the initial and final quantities (mol) of vanillin, respectively, and C_i is the quantity (mol) of the identified product. In addition, 0-Os, 1-Os, and 2-Os denote molecules containing no oxygen atom, one oxygen atom, and two oxygen atoms, respectively.

3. Results and discussion

3.1. TEM, SEM, and XRD

Ru nanoparticles cogelled with alumina (Ru@Al) were prepared using an in-situ alumina gelation method in the presence of Ru colloids stabilized with PVP (Figs. 1(a) and S1(a)). Other alumina-supported Ru catalysts were synthesized by a modified impregnation method exhibiting Ru nanoparticles clearly exposed on alumina supports: Ru/FreeAl (Figs. 1 and S1(b)), Ru/AeroAl (Figs. 1 and S1(c)) and Ru/γ-Al₂O₃ (Figs. 1 and S1(d)) using FreeAl (alumina prepared by the same method used for the synthesis of Ru@Al but in the absence of Ru), AeroAl (alumina aerogel), and γ-Al₂O₃ (commercially available γ-alumina) as supports, respectively. Bright-field TEM (BF-TEM) did not clearly observe the Ru particles (Fig. 1(a)), but HAADF-STEM exhibited the formation of Ru particles on the alumina support (Fig. S1(a)). Based on these electron micrographs, it is hypothesized that numerous Ru

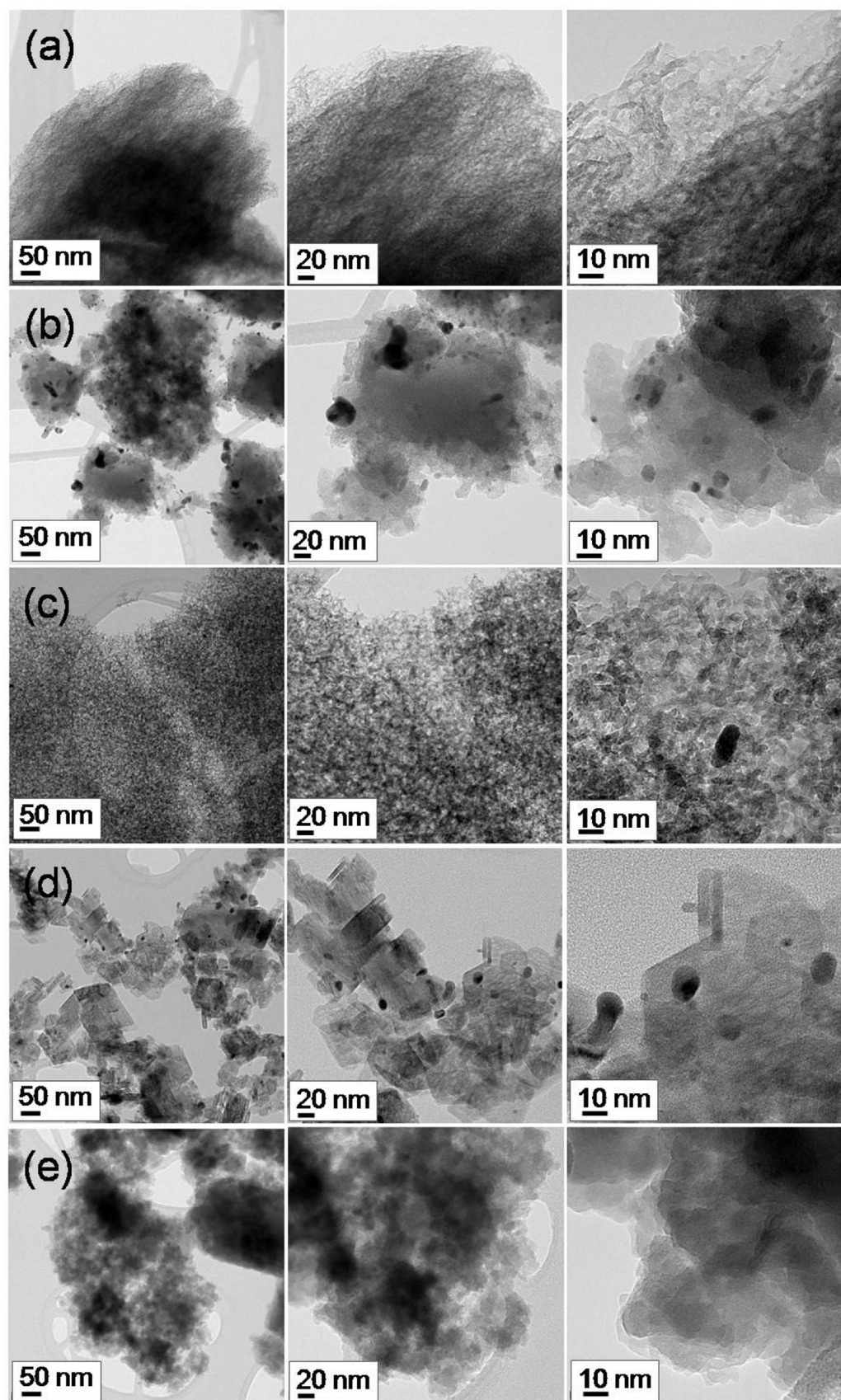


Fig. 1. BF-TEM images of (a) Ru@Al, (b) Ru/FreeAl, (c) Ru/AeroAl, (d) Ru/ γ -Al₂O₃, and (e) FreeAl.

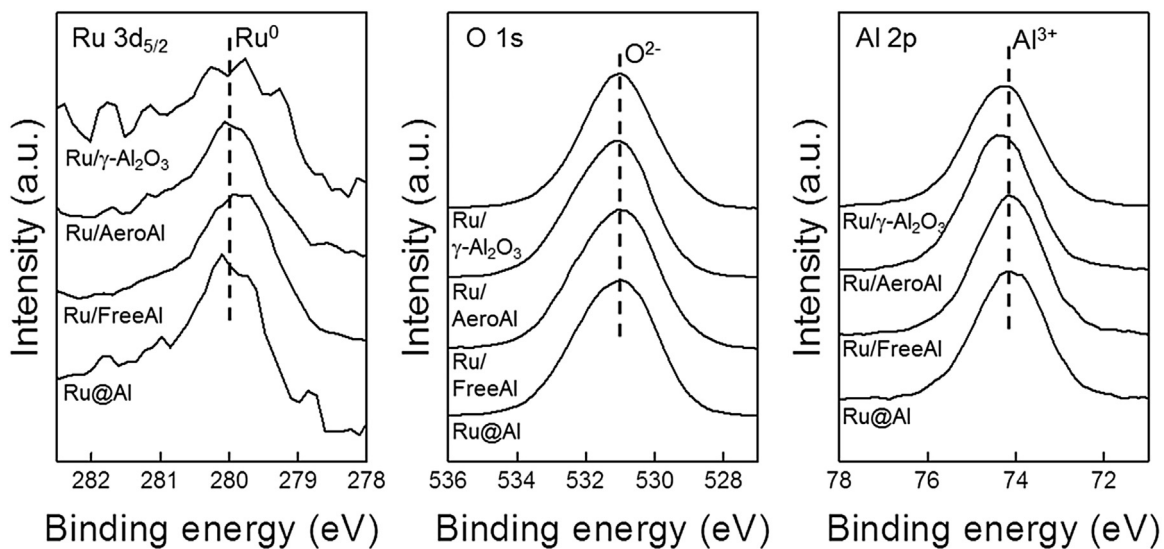


Fig. 2. XPS results of alumina-supported Ru catalysts.

nanoparticles in the Ru@Al may be partially or fully wrapped inside the space between the alumina support particles because the alumina in Ru@Al was formed by a sol-gel process in the presence of PVP-stabilized Ru nanoparticles [20].

SEM observations with EDX mapping exhibited that the catalysts in this study were composed of only Ru, Al, and O (Fig. S2). The elemental compositions on the catalyst surface indicated that the fractions of Ru were 2.2–2.6 wt% for Ru@Al, Ru/FreeAl, and Ru/AeroAl, not significantly different from the introductory loading of Ru (2 wt%), whereas Ru/γ-Al₂O₃ exhibited 5.0 wt% Ru (Table S2). Because the alumina supports of Ru@Al, Ru/FreeAl, and Ru/AeroAl are nanometer-scaled structures compared to the thick nonporous alumina of Ru/γ-Al₂O₃, the alumina of Ru/γ-Al₂O₃ appeared at lower amounts in the EDX measurements and the superficial loading of Ru for Ru/γ-Al₂O₃ increased. The XRD results for Ru@Al, Ru/FreeAl, Ru/AeroAl, and Ru/γ-Al₂O₃ confirmed the formation of metallic hexagonal Ru particles (Fig. S3). Note that Ru/γ-Al₂O₃ exhibited γ-Al₂O₃ [28] and boehmite crystal structures [29], and the alumina supports of other catalysts were amorphous.

3.2. N₂-Physisorption

The N₂-physisorption results also demonstrated the formation of possible interparticle spaces between alumina particles for Ru@Al (Table 1 and Fig. S4). BJH and *t*-plot analyses indicate that Ru@Al did not contain micropores, instead creating only mesopores of approximately 4 nm. As previously observed for alumina-supported Pt catalysts [20], the alumina particles must be nonporous, and the observed mesopores appeared to be created by the interparticle space. Other catalysts exhibited similar BET surface areas ranging from 262 to 322 m²/g, except for Ru/γ-Al₂O₃ (61 m²/g). Ru/AeroAl had a pore width of 5–17 nm, but FreeAl, Ru/FreeAl, and Ru/γ-Al₂O₃ did not exhibit well-defined mesoporous structures. From the *t*-plot analyses, a large micropore surface area was observed for FreeAl and Ru/FreeAl, whereas a negligible micropore surface area was observed for Ru@Al. Ru/AeroAl and Ru/γ-Al₂O₃ exhibited a smaller micropore surface area compared to those of Ru@Al and FreeAl.

3.3. XPS

The XPS results of the prepared catalysts indicate that the electronic structures of Ru and Al₂O₃ were not significantly different

for each catalyst prepared with different methods not affecting the catalytic activity (Fig. 2). Because the Ru 3d_{3/2} peak was overlapped with the strong C 1s peak, Ru 3d_{5/2} was studied in an effort to understand the electronic states of Ru. The formation of Ru⁰ was confirmed for all catalysts, and cationic Ru peaks were not clearly observed. In addition, negligible differences in the Al 2p exhibiting Al³⁺ peaks were observed except for Ru/AeroAl, whose Al³⁺ was slightly more cationic with higher binding energy by ~0.2 eV. The O 1s peaks did not exhibit a significant difference between the catalysts.

3.4. CO-chemisorption and H₂-TPD

The Ru dispersions of catalysts were measured using CO-chemisorption, which exhibited [CO]/[Ru]=0.162–0.266 (mol/mol) (Table S3). Ru@Al and Ru/γ-Al₂O₃ exhibited lower [CO]/[Ru] values of 0.162 and 0.164, respectively, while Ru/FreeAl and Ru/AeroAl exhibited higher corresponding [CO]/[Ru] values of 0.266 and 0.264. In addition, we attempted H₂-TPD to understand the bonding of H₂ or H on the catalyst surface (Fig. S5). Ru@Al and Ru/FreeAl exhibited similar desorption behaviors, indicating major desorption curves at 250–600 °C or higher. Ru/AeroAl exhibited a strong desorption peak at 400–500 °C. Ru/γ-Al₂O₃ exhibited a broad desorption peak at 350–600 °C. These observations indicate that the adsorption of H atoms on the Ru surface was weaker for Ru@Al and Ru/FreeAl and stronger for Ru/AeroAl and Ru/γ-Al₂O₃. Based on these observations, the hydrogenation activities of Ru@Al and Ru/FreeAl may be different from those of Ru/AeroAl and Ru/γ-Al₂O₃ affecting the catalytic hydrogenation and hydrodeoxygenation activity.

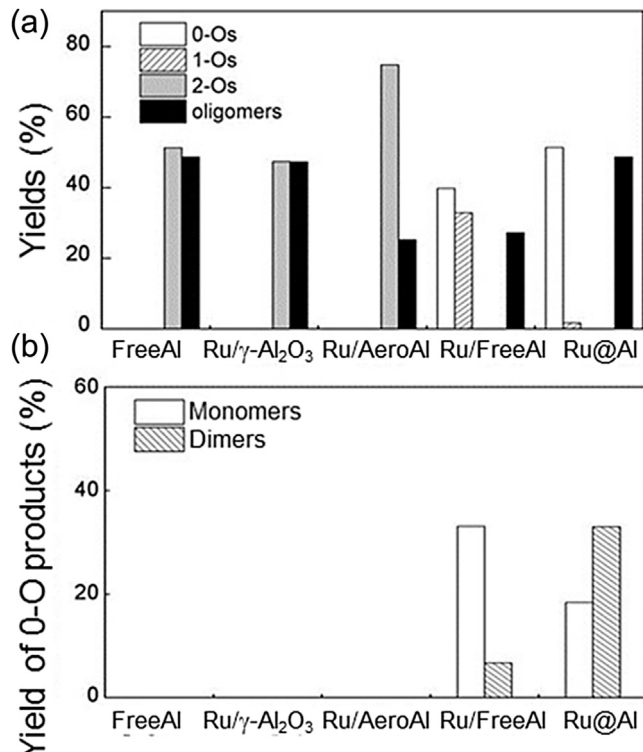
3.5. NH₃-TPD/MS

In the range of 100–900 °C from the NH₃-TPD results (Fig. S6), the formation of water, carbon monoxide, and carbon dioxide was observed as well as desorbed ammonia. The desorption of water at a high temperature can be attributed to the dehydration of the alumina surface, and carbon monoxide and carbon dioxide may form from the residual carbon on the catalyst surface. Based on these observations, we measured the acid concentrations using the TCD curve at 100–400 °C (Table 1), which exhibited ammonia and a small shoulder of carbon monoxide at 300 °C. The quantities of acid sites of Ru@Al and Ru/FreeAl were nearly identical

Table 1

BET surface areas, pore volumes, and acid site concentrations of supported Ru catalysts.

Catalyst	BET surface area (m^2/g)	Pore volume (cm^3/g) ^a	Micropore surface area (m^2/g) ^b	Acid site concentration (mmol/g) ^c
Ru@Al, fresh	262	0.3	~0	0.56
Ru@Al, spent	82	0.2	~0	0.27
Ru/FreeAl, fresh	284	0.2	256	0.56
Ru/AeroAl, fresh	322	1.3	15	0.50
Ru/ γ -Al ₂ O ₃ , fresh	61	0.2	27	0.19
FreeAl, fresh	237	0.2	207	–

^a Pore volumes were calculated using the BJH desorption pore size distributions measured by N₂-physisorption.^b Measured by a *t*-plot analysis using the N₂-physisorption results.^c Quantity of acid sites measured using NH₃ desorbed at 100–400 °C using the NH₃-TPD/MS results.**Fig. 3.** (a) Catalysis results and (b) product distribution of the HDO of vanillin using Ru@Al, Ru/FreeAl, Ru/AeroAl, and Ru/ γ -Al₂O₃. The reaction was performed with vanillin (1.8 mmol), water (30 mL) and a catalyst (50 mg) at a H₂ pressure of 40 bar (measured at room temperature) and at 270 °C for 2 h.

(0.56 mmol/g for both), whereas Ru/AeroAl exhibited a slightly lower value (0.50 mmol/g), with Ru/ γ -Al₂O₃ exhibiting the lowest value (0.19 mmol/g).

3.6. Catalysis

The hydrodeoxygenation (HDO) of vanillin was performed using the alumina-supported Ru catalysts prepared in this study (Fig. 3 and Table S4), with Ru@Al exhibiting good condensation and hydrodeoxygenation activities. The compounds containing no oxygen atoms (0-Os), those containing only one oxygen atom (1-Os), those containing two oxygen atoms (2-Os), and high-molecular-weight oligomers were produced from the three-oxygen-containing vanillin (Fig. S7). The HDO using Ru@Al produced the largest quantity of 0-Os (51.4%), including 1-cyclohexylmethyl-2-methyl-cyclohexane (19.0%) and 1,1'-methylenebis(cyclohexane) (7.1%), which can be obtained by the condensation of two phenolic monomers, as well as methylcyclohexane (12.8%), exhibiting an oxygen removal of 52.5%. The

reaction using Ru/FreeAl also exhibited a good oxygen removal (61.7%), although it produced less 0-Os (39.8% vs. 51.4% for Ru@Al) and more 1-Os (32.9% vs. 1.7% for Ru@Al). The other alumina-supported Ru catalysts, in this case Ru/ γ -Al₂O₃ and Ru/AeroAl, exhibited lower oxygen removals of 15.8% for Ru/ γ -Al₂O₃ and 24.9% for Ru/AeroAl, without producing 0-Os and 1-Os. The Ru-free FreeAl exhibited very low catalytic activity, with oxygen removal of 17.1%, and it did not produce 0-Os or 1-Os. The reactions using FreeAl and Ru/ γ -Al₂O₃ produced large quantities of oligomers with the poor hydrodeoxygenation of vanillin.

The effects of reaction temperature on the catalysis results were also investigated using Ru@Al at 210–300 °C (Fig. S8). With increasing reaction temperature from 210 to 270 °C, the selectivities to 0-Os and oligomers increased from 15.0 to 55.2% and 20.4–37.5%, respectively, while those of 1-Os and 2-Os decreased from 31.5 to 4.4% and 31.6–2.9%, respectively. The decreasing activity at 300 °C was probably attributed to the formation of non-condensable gases through catalytic cracking of vanillin or the formation of catalyst-poisoning char at high temperature (Fig. S8(a)). It should be noted that Ru@Al produced significantly larger quantity of dimeric deoxygenates than monomeric ones at all temperature range (Fig. S8(b)).

3.7. Reaction pathway

The different activities of the catalysts were further studied by devising the probable reaction pathways (Fig. 4), which indicated that improved condensation activity is required to produce dimeric hydrocarbons. As reported in the literature [22,23], vanillin alcohol (2) and *p*-creosol (3) are formed by the conversion of vanillin. The conversion of vanillin (1) to *p*-creosol occurred through (i) the hydrogenation of vanillin to vanillin alcohol and (ii) the hydrogenolysis of the C–O bond. Monomeric oxygenates can be hydrodeoxygenated to cycloalkanes, including cyclohexane and methylcyclohexane. In addition to the monomeric compounds, dimeric compounds were formed by the condensation of the reactants and intermediates [30]. Vanillin alcohol and *p*-creosol were condensed to form 5-(4-hydroxy-3-methoxybenzyl)-2-methoxy-4-methylphenol (9) and 2-(4-hydroxy-3-methoxybenzyl)-6-methoxy-4-methylphenol (11), which were further hydrogenated to form 1-(cyclohexylmethyl)-2-methylcyclohexane (10) and hydrogenolized to form 1-(cyclohexylmethyl)-3-methylcyclohexane (12), respectively. The condensation of vanillin alcohol and guaiacol formed 4-(3-hydroxy-4-methoxybenzyl)-2-methoxyphenol (7), which was further hydrogenated and hydrogenolized to form 1,1'-methylenebis(cyclohexane) (8). These reaction pathways indicated that the production of deoxygenated monomeric hydrocarbons must arise because of hydrogenation and hydrogenolysis with less condensation, whereas the production of deoxygenated dimeric hydrocarbons requires condensation in addition to hydrogenation and hydrogenolysis. From these catalysis results, Ru@Al and Ru/FreeAl

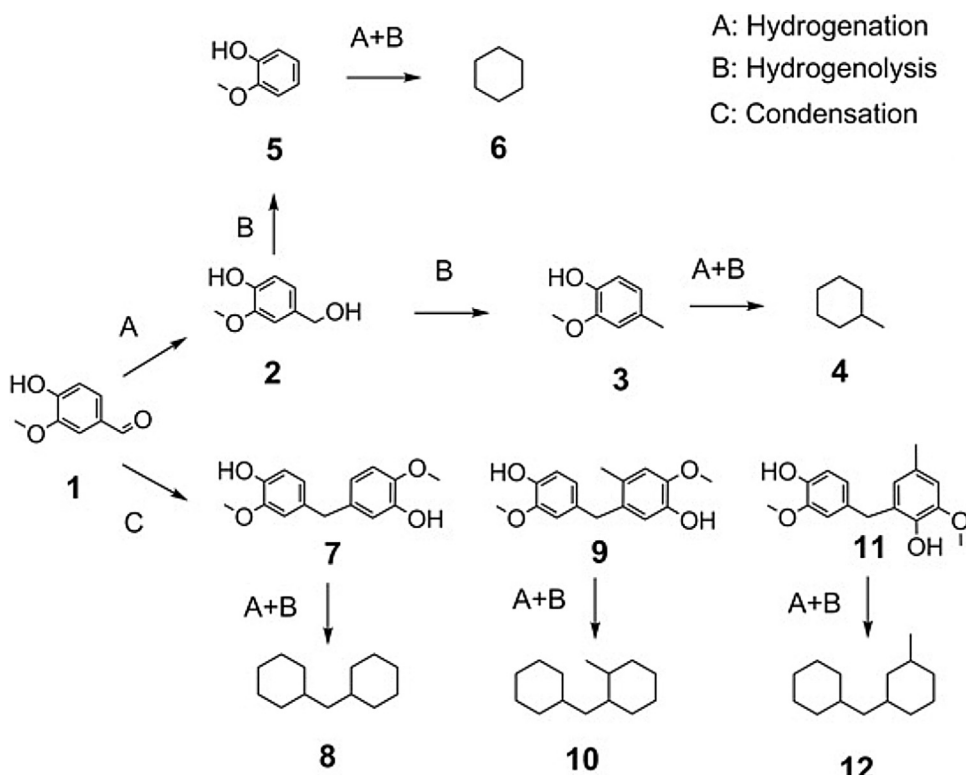


Fig. 4. Reaction pathways for the HDO of vanillin.

produced a significantly large quantities of dimeric deoxygenates, while FreeAl, Ru/ γ -Al₂O₃, and Ru/AeroAl preferentially produced 2-Os and oligomers without 0-Os and 1-Os. Ru@Al exhibited more dimeric 0-Os, including 1,1'-methylenebis(cyclohexane) and 1-(cyclohexylmethyl)cyclohexane, compared to Ru/FreeAl.

Based on these observations, the structures of the catalysts were studied in more depth in an effort to understand how the condensation and hydrodeoxygenation activities of Ru@Al were improved. The generally known descriptors including the metal dispersion, the pore structure, and the acidity were investigated in this study (Fig. S9). First, the acidity of the catalysts was investigated using NH₃-TPD/MS (Table 1 and Fig. S6) because the HDO activity of bifunctional catalysts may depend on their acidity [11]. Although highly active Ru@Al and Ru/FreeAl exhibited more acid sites compared to Ru/ γ -Al₂O₃ and Ru/AeroAl, the deoxygenation activity was not fully dependent on the quantity of the acid sites (Fig. S9(a)).

Second, the pore structure of the catalysts was investigated, indicating that the BET surface area did not determine the catalytic deoxygenation activity (Fig. S9(b)). Ru/AeroAl with the largest BET surface area and well-developed mesopores exhibited a smaller oxygen removal, while Ru/FreeAl and Ru@Al with smaller BET surface areas exhibited greater oxygen removals.

Third, the quantity of active-surface Ru atoms measured by CO-chemisorption (Table S3) was correlated with the catalytic activity (Fig. S9(c)). Active Ru@Al and poor Ru/ γ -Al₂O₃ exhibited the fewest surface Ru atoms, while poor Ru/AeroAl and active Ru/FreeAl exhibited large quantities of surface Ru atoms. These observations indicate that the quantity of Ru active sites did not determine the hydrogenation or hydrodeoxygenation activity. Note that the XRD results of supported Ru catalysts exhibited the diffractions of metallic hexagonal Ru but no other Ru derivatives (Fig. S3), while the diameters of the Ru nanoparticles, as measured by the Scherrer equation using Ru(101) at $2\theta = 44^\circ$, were similar at 10.8, 11.7, 12.8, and 11.9 nm for Ru@Al, Ru/FreeAl, Ru/AeroAl and Ru/ γ -Al₂O₃, respectively [31]. These observations exclude the possible

adjustment of the catalytic activity by the size-dependent morphology change.

As discussed above, the generally accepted descriptors for the supported noble metal catalysts did not determine the deoxygenation activity in this study. Another factor to consider with regard to the catalytic activity of Ru@Al, the morphology of the supports, was introduced. As depicted in Fig. 3(b) for the fully deoxygenated products, the HDO of vanillin on Ru@Al preferentially produced dimers (33.0%) rather than monomers (18.4%). In contrast, the reaction on Ru/FreeAl produced monomers (33.1%) instead of dimers (6.7%). The observed selectivity can be attributed to the different structures of the catalysts and thus the adjustment of the reaction pathway (Figs. 4 and 5). Because Ru@Al was prepared by mixing Ru colloids with alumina precursors, the nanoparticles can be surrounded by Al₂O₃ nanostructures, as previously suggested [20,32]. Based on the reaction pathway of Fig. 4, the improved condensation must be attributed to the preferred reaction on alumina before the reactants were hydrogenated or hydrodeoxygenated on Ru (Fig. 5(b)). Because the hydrogen-adsorbing Ru nanoparticles were surrounded three-dimensionally by Al₂O₃, the phenolic monomer reactants were adsorbed onto the Al₂O₃ surface before they could reach the hydrogen-adsorbed Ru, after which they were dimerized prior to the reaction with the hydrogen atoms. The dimeric compounds were further oligomerized or diffused to adjacent Ru surfaces, becoming hydrodeoxygenated to dimeric 0-Os. The reaction on two control catalysts, Ru/FreeAl and Ru-free FreeAl, was performed to confirm the reaction results. The reactants on Ru/FreeAl were quickly hydrodeoxygenated before they were dimerized because Ru particles appeared to be exposed on the bulk surface of FreeAl, improving the hydrogen-involved reaction of the phenolic reactants (Fig. 5(a)); the formation of deoxygenated dimers was not preferred, and *p*-creosol and guaiacol were subsequently converted to methylcyclohexane (**4**) and cyclohexane (**6**), respectively. FreeAl without Ru particles cannot initiate hydrogenation because hydrogen atoms cannot adsorb onto the

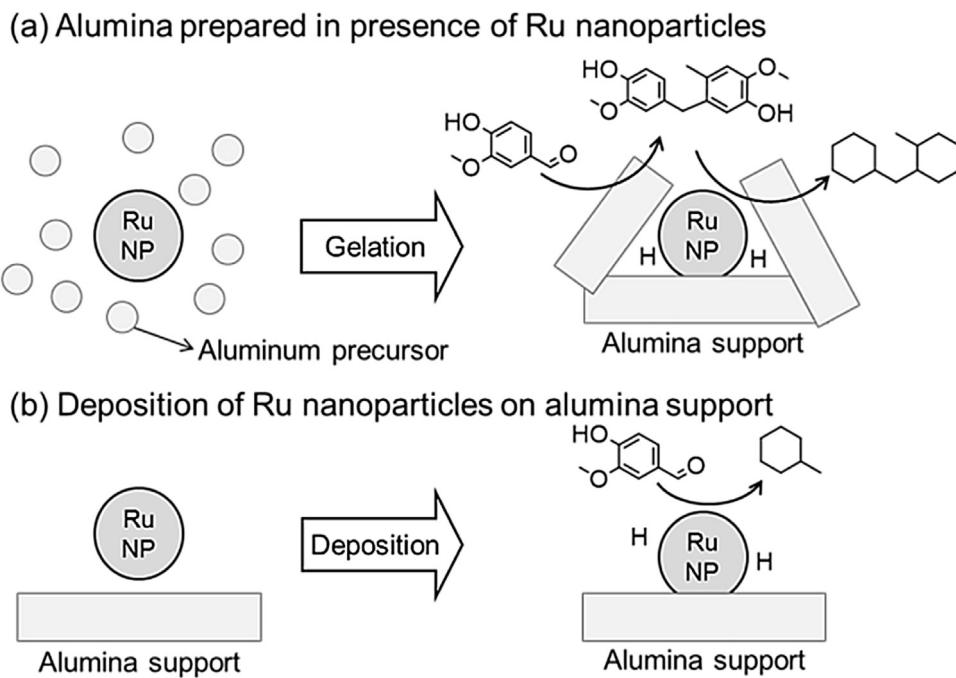


Fig. 5. Suggested catalysis on (a) Ru@Al and (b) Ru/FreeAl.

catalyst surface. Instead, phenolic compounds can be dimerized or oligomerized on the alumina surface to produce the oxygenated aromatic dimers and oligomers.

The important synergy of Ru and alumina during the catalysis on Ru@Al was further observed with the reaction using spent Ru@Al (Fig. S10 and Table S5), which indicates that the Al_2O_3 structure is important to determine the catalytic activity of Ru@Al. While significant deactivation was observed for the spent Ru@Al exhibiting poor deoxygenation activity, the sintering of Ru nanoparticles was not observed, with $[\text{CO}]/[\text{Ru}] = 0.161$ (mol/mol) for the spent Ru@Al compared to 0.162 (mol/mol) for the fresh Ru@Al. In contrast to the stable Ru nanoparticles, the transformation of alumina was distinct. The XRD of the spent Ru@Al exhibited the formation of boehmite from the amorphous alumina of fresh Ru@Al (Fig. S11). The formation of the bulk crystal structure from amorphous structure requires the transition of Al and O atoms to build an ordered structure leading to the significant transformation of alumina. The N_2 -physisorption exhibited a decreased BET surface area for spent Ru@Al because of the significant change in the nanostructures, which is most likely attributed to the phase transition of amorphous alumina to boehmite (Fig. S12). The NH_3 -TPD/MS exhibited an approximately 50% decrease of the acid concentrations for the spent Ru@Al, which, however, cannot explain the almost complete loss of deactivation activity (Fig. S13). These observations indicate that the nanostructure of Al_2O_3 affects the catalytic condensation and deoxygenation activity as suggested in Fig. 5, while the transformation of the alumina nanostructure deactivates the Ru@Al catalyst.

4. Conclusion

With the nanoparticle-alumina geometry prepared by a simple one-pot synthesis method, catalysis modification from hydrodeoxygengation on conventional alumina-supported Ru to the condensation-then-hydrodeoxygengation reaction on Ru@Al improved the yields of high-carbon-number hydrocarbons. The catalysis process was mostly adjusted by three-dimensional structures of Ru wrapped by alumina, which initiated condensation on

the alumina surface before the hydrogen-involved reaction on the Ru surface occurred. The observations in this study can be used for the production of high-energy-density fuels during the upgrading of biomass-thermolysis oils.

Acknowledgements

This work was supported by the National Research Council of Science & Technology (NST) grant by the Korea government (MSIP) (No. CAP-11-04-KIST). This work was also supported by the Korea Institute of Science and Technology (KIST) institutional program (2E26550).

Appendix A. Supplementary data

Supplementary data associated with this article can be found, in the online version, at <http://dx.doi.org/10.1016/j.apcata.2016.07.012>.

References

- [1] S. Czernik, A.V. Bridgwater, Energy Fuels 18 (2004) 590–598.
- [2] P. McKendry, Bioresour. Technol. 83 (2002) 47–54.
- [3] A.V. Bridgwater, Biomass Bioenergy 38 (2012) 68–94.
- [4] T.P. Vispute, H. Zhang, A. Sanna, R. Xiao, G.W. Huber, Science 330 (2010) 1222–1227.
- [5] M. Saidi, F. Samimi, D. Karimpourfard, T. Nimmanwudipong, B.C. Gates, M.R. Rahimpour, Energy Environ. Sci. 7 (2014) 103–129.
- [6] G.W. Huber, S. Iborra, A. Corma, Chem. Rev. 106 (2006) 4044–4098.
- [7] I. Yati, M. Yeom, J.-W. Choi, H. Choo, D.J. Suh, J.-M. Ha, Appl. Catal. A 495 (2015) 200–205.
- [8] J.S. Yoon, Y. Lee, J. Ryu, Y.-A. Kim, E.D. Park, J.-W. Choi, J.-M. Ha, D.J. Suh, H. Lee, Appl. Catal. B 142–143 (2013) 668–676.
- [9] C. Zhao, W. Song, J.A. Lercher, ACS Catal. 2 (2012) 2714–2723.
- [10] A. Corma, O. de la Torre, M. Renz, Energy Environ. Sci. 5 (2012) 6328–6344.
- [11] C.R. Lee, J.S. Yoon, Y.-W. Suh, J.-W. Choi, J.-M. Ha, D.J. Suh, Y.-K. Park, Catal. Commun. 17 (2012) 54–58.
- [12] A.A. Dwiatmoko, S. Lee, H.C. Ham, J.-W. Choi, D.J. Suh, J.-M. Ha, ACS Catal. 5 (2015) 433–437.
- [13] W. Zhang, J. Chen, R. Liu, S. Wang, L. Chen, K. Li, ACS Sustain. Chem. Eng. 2 (2014) 683–691.
- [14] A. Foster, P.M. Do, R. Lobo, Top. Catal. 55 (2012) 118–128.
- [15] M.S. Zanuttini, C.D. Lago, C.A. Querini, M.A. Peralta, Catal. Today 213 (2013) 9–17.

- [16] J.S. Yoon, J.W. Choi, D.J. Suh, K. Lee, H. Lee, J.M. Ha, *ChemCatChem* 7 (2015) 2669–2674.
- [17] J. Zhang, H. Asakura, J. van Rijn, J. Yang, P. Duchesne, B. Zhang, X. Chen, P. Zhang, M. Saeyns, N. Yan, *Green Chem.* 16 (2014) 2432–2437.
- [18] J. Zhang, J. Teo, X. Chen, H. Asakura, T. Tanaka, K. Teramura, N. Yan, *ACS Catal.* 4 (2014) 1574–1583.
- [19] H. Konnerth, J. Zhang, D. Ma, M.H.G. Prechtl, N. Yan, *Chem. Eng. Sci.* 123 (2015) 155–163.
- [20] I. Yati, M. Ridwan, G.E. Jeong, Y. Lee, J.-W. Choi, C.W. Yoon, D.J. Suh, J.-M. Ha, *Catal. Commun.* 56 (2014) 11–16.
- [21] S. Crossley, J. Faria, M. Shen, D.E. Resasco, *Science* 327 (2010) 68–72.
- [22] Z. Zhu, H. Tan, J. Wang, S. Yu, K. Zhou, *Green Chem.* 16 (2014) 2636–2643.
- [23] X. Xu, Y. Li, Y. Gong, P. Zhang, H. Li, Y. Wang, *J. Am. Chem. Soc.* 134 (2012) 16987–16990.
- [24] X. Yang, Y. Liang, Y. Cheng, W. Song, X. Wang, Z. Wang, J. Qiu, *Catal. Commun.* 47 (2014) 28–31.
- [25] X. Yang, Y. Liang, X. Zhao, Y. Song, L. Hu, X. Wang, Z. Wang, J. Qiu, *RSC Adv.* 4 (2014) 31932–31936.
- [26] A.A. Dwiatmoko, L. Zhou, I. Kim, J.-W. Choi, D.J. Suh, J.-M. Ha, *Catal. Today* 265 (2016) 192–198.
- [27] M. Sadakiyo, M. Kon-no, K. Sato, K. Nagaoka, H. Kasai, K. Kato, M. Yamauchi, *Dalton Trans.* 43 (2014) 11295–11298.
- [28] E.J.W. Verwey, *Z. Kristallogr.* 317 (1935).
- [29] R.J. Hill, *Clays Clay Miner.* 29 (1981) 435–445.
- [30] J. Hemmingson, G. Leary, *Aust. J. Chem.* 33 (1980) 917–925.
- [31] B.D. Cullity, S.R. Stock, *Elements of X-ray Diffraction*, Prentice Hall, Reading, Massachusetts, 2001.
- [32] Z. He, X. Wang, *Catal. Sust. Energy* 1 (2012) 28.